Admittance-Based Controller Design for Physical Human–Robot Interaction in the Constrained Task Space

Wei He, *Senior Member, IEEE*, Chengqian Xue, Xinbo Yu, *Student Member, IEEE*, Zhijun Li, *Senior Member, IEEE*, and Chenguang Yang, *Senior Member, IEEE*

***Abstract*— In this article, an admittance-based controller for physical human–robot interaction (pHRI) is presented to perform the coordinated operation in the constrained task space. An admittance model and a soft saturation function are employed to generate a differentiable reference trajectory to ensure that the end-effector motion of the manipulator complies with the human operation and avoids collision with surroundings. Then, an adaptive neural network (NN) controller involving integral barrier Lyapunov function (IBLF) is designed to deal with tracking issues. Meanwhile, the controller can guarantee the end-effector of the manipulator limited in the constrained task space. A learning method based on the radial basis function NN (RBFNN) is involved in controller design to compensate for the dynamic uncertainties and improve tracking performance. The IBLF method is provided to prevent violations of the constrained task space. We prove that all states of the closed-loop system are semiglobally uniformly ultimately bounded (SGUUB) by utilizing the Lyapunov stability principles. At last, the effectiveness of the proposed algorithm is verified on a Baxter robot experiment platform.**

***Note to Practitioners*—This work is motivated by the neglect of safety in existing controller design in physical human–robot interaction (pHRI), which exists in industry and services, such as assembly and medical care. It is considerably required in the controller design for rigorously handling constraints. Therefore, in this article, we propose a novel admittance-based human–robot interaction controller. The developed controller has the following functionalities: 1) ensuring reference trajectory remaining in the constrained task space: a differentiable reference trajectory is shaped by the desired admittance model and a soft saturation function; 2) solving uncertainties of robotic dynamics: a learning approach based on radial basis function neural network (RBFNN) is involved in controller design; and 3) ensuring the end-effector of the manipulator remaining in the constrained task space: different from other barrier Lyapunov function (BLF), integral BLF (IBLF) is proposed to constrain system output directly rather than tracking error, which may be more convenient for controller designers. The controller can be potentially applied in many areas. First, it can be used in the rehabilitation robot to avoid injuring the patient by limiting the motion. Second, it can ensure the end-effector of the industrial manipulator in a prescribed task region. In some industrial tasks, dangerous or damageable tools are mounted on the end-effector, and it will hurt humans and bring damage to the robot when the end-effector is out of the prescribed task region. Third, it may bring a new idea to the designed controller for avoiding collisions in pHRI when collisions occur in the prescribed trajectory of end-effector.**

***Index Terms*— Adaptive neural network (NN) control, admittance control, integral barrier Lyapunov function (IBLF), motion constraint, physical human–robot interaction (pHRI).**

Manuscript received December 6, 2019; revised January 31, 2020; accepted March 1, 2020. This article was recommended for publication by Associate Editor Z. Xiong and Editor Q. Zhao upon evaluation of the reviewers' comments. This work was supported in part by the National Natural Science Foundation of China under Grant 61933001 and Grant 61873298, in part by the Joint Funds of Equipment Pre-Research and Ministry of Education of China under Grant 6141A02033339, in part by the Beijing Top Discipline for Artificial Intelligent Science and Engineering, USTB, and in part by the National Key Research and Development Program of China under Grant 2017YFB1302302 and Grant 2018YFC2001600. *(Corresponding author: Wei He.)*

Wei He, Chengqian Xue, and Xinbo Yu are with the Institute of Artificial Intelligence, University of Science and Technology Beijing, Beijing 100083, China, and also with the Key Laboratory of Knowledge Automation for Industrial Processes of Ministry of Education, School of Automation and Electrical Engineering, University of Science and Technology Beijing, Beijing 100083, China (e-mail: weihe@ieee.org).

Zhijun Li is with the Department of Automation, University of Science and Technology of China, Hefei 230026, China.

Chenguang Yang is with the Bristol Robotics Laboratory, University of the West of England, Bristol BS16 1QY, U.K.

Color versions of one or more of the figures in this article are available online at http://ieeexplore.ieee.org.

Digital Object Identifier 10.1109/TASE.2020.2983225

I. Introduction

In RECENT years, as robots transition from industrial applications to service areas, social robots become more and more significant in our daily life [1]–[6]. In view of security of physical human–robot interaction (pHRI), the significance of methods for interaction control is increasing [7]–[10]. Control design in pHRI tasks is much more complicated than that in noninteractive scenarios. Like rehabilitation robots, they should not only guide the motion of patient limb but also comply with forces exerted by the patient for compliance. Only the motion control method may not meet requirements for complex tasks in pHRI.

Considering a classical pHRI scenario as in Fig. 1, human and robot perform coordinated operation in the constrained task space. Robot can be a rehabilitation robot or an industrial manipulator, and human operates the end-effector of robot for recovering in rehabilitation or performing some tasks collaboratively. The main difficulty in such tasks lies in controlling manipulators complying with the operator and constraining it in the predefined task space simultaneously. In order to solve issues of compliance in pHRI, various control methods

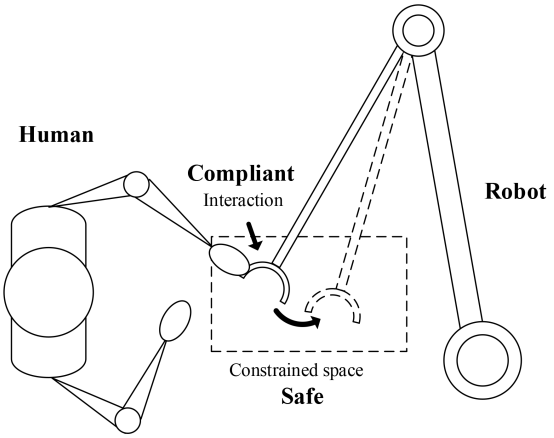

Fig. 1. Typical human–robot interactive scenario in the constrained task space.

have been proposed. In [11], hybrid position/force control is proposed first to achieve compliant interaction by controlling the terminal position and contact force simultaneously. Then, some studies have made extensions to this control scheme for solving pHRI problems [12]–[14]. The impedance control is proposed first by Hogan [15] to express the relationships between the contact force and state in a prescribed impedance model. Compared with hybrid force/position control, impedance control does not require control transitions between contact and noncontact situations and has a better performance in robustness. Depending on the causality of the controller, there are two ways to implement impedance control, which are often referred to as impedance control and admittance control in the literature [16]. In recent years, impedance control and admittance control have become two of the most efficient control methods in pHRI [17]–[19]. In [20], an adaptive admittance control is proposed to enable humans to interact with a robot whose behavior is like a prescribed admittance model under control design. In [21], an adaptive admittance control method without external sensors is proposed to enable pHRI for manipulators in the industrial environment. In [22], a learning impedance controller is proposed to control the robotic system following a given impedance model and achieve interactive control objective for pHRI. In [23], a unified torque–impedance controller is proposed for the pneumatically actuated antagonistic manipulator joint. The controller has good performance for both operations of trajectory tracking and torque control and can handle the contact loss fast and accurately in pHRI. In [24], a hybrid passivity-based Cartesian force/impedance controller is proposed for robots to realize the accurate force tracking, handle unexpected contact loss, and avoid chattering behavior. Although admittance control can improve the performance in pHRI, such a method does not guarantee operational security since admittance control can only regulate interactive force without constraining the position of manipulators. Emphatically, a major obstacle in the field of application is that position constraints are not considered in the abovementioned design. Therefore, position constraints should be considered in the control design to ensure security during pHRI.

Due to actual physical device limitations [25]–[28], system performance, and safety requirements [29]–[32], output or states in most systems should be constrained in practice [33]–[37]. Therefore, it is considerably significant to maintain system's outputs in the desired constraints [38]–[41]. For a nonlinear system of manipulators, output constraints can be regarded as position constraints. In recent years, the barrier Lyapunov function (BLF) is proposed for solving output constrained issues in complex systems [42]. In [43], an asymmetric time-varying BLF is employed in strict feedback nonlinear systems to ensure the time-varying output constraints. In [44], an adaptive control scheme is developed for nonlinear stochastic systems with unknown parameters. All the states of the systems are required to be constrained in bounded compact sets with log-type BLF. In [45], the output constraint problem of uncertain nonstrict-feedback systems is handled by utilizing a BLF. In [46], tan-type BLF is used to maintain the output in constraints under systematic control design for strict-feedback nonlinear systems. In [47], the tan-type BLF is incorporated with a novel fault-tolerant leader–follower formation control scheme to ensure the angle constraints. Compared with the conventional log- and tan-type BLFs, controllers with a novel integral BLF (IBLF) can constrain state signals directly, rather than error signals [48]. From the engineering point of view, the initial states of robots can be relaxed to the whole constrained space. Therefore, in this article, IBLF is used to guarantee the end-effector of the manipulator in the constrained task space.

The uncertainty of manipulator dynamics cannot be ignored in robot controller design [49]–[51]. To solve uncertainty issues, neural networks (NNs) are widely used to estimate unknown parameters of the system in the literature [52]–[55]. In [56], adaptive NNs are used to approximate uncertainties in rehabilitation robot dynamics and adapt the interactions between robot and patient. In [57], adaptive NN control is used to research the multirate networked industrial process control problem in double-layer architectures. In [58], a fuzzy NN learning algorithm is proposed to identify the uncertain plant model, and the tracking performance of the controller is guaranteed. Compared with other NN control methods [59], radial basis function NN (RBFNN) performs better in approximating unknown model of a nonlinear function because it is a local approximation network with simple structure and fast convergence speed.

Based on the abovementioned discussion, in this article, an IBLF and a soft saturation function are jointly designed to guarantee the manipulator end-effector within the constrained task space in two lines: controller design and path planning. An admittance-based controller for pHRI, involving in IBLF and RBFNN learning method, is designed for solving uncertainties in dynamics. Meanwhile, the controller can guarantee the end-effector of the manipulator in the constrained task space and improve the compliance of interaction. Compared with existing works, the main contributions of this article include the following.

1) Compared with traditional admittance control [60], a soft saturation function is employed to further shape the tracking reference trajectory that generates from the

desired admittance model, and the reference trajectory will be ensured in the constrained task space.

2) A learning method based on RBFNN is proposed to approximate uncertainties in manipulator dynamics, and an adaptive NN admittance controller is designed to track the reference trajectory precisely.
3) Compared with common BLF, such as log- and tan-type BLFs [43]–[47], IBLF is used to constrain output signals directly, rather than error signals. From the engineering point of view, setting proper position constrained boundary is more effective and convenient in a pHRI scenario. When we use other BLF methods considering constraining position error, unknown time-varying human reference trajectory may generate a time-varying constrained boundary, which may be out of our desired constrained task region. Therefore, setting the prescribed position constrained boundary is required in pHRI applications to guarantee the manipulator performing a coordinated operation within the constrained task space.

The rest of this article is organized as follows. In Section II, the system dynamic model and preliminaries are demonstrated. In Section III, constrained space and reference trajectory are shaped, and an adaptive NN admittance controller is designed. In Section IV, experiments are designed to verify the effectiveness of the proposed method. In Section V, we summarize research results.

II. Preliminarlies and Problem Formulation

A. Problem Formulation

A typical pHRI in the constrained task space is shown in Fig. 1. The motion of manipulator needs to comply with human motion, and excessive interaction force brings uncomfortable feelings to human. Meanwhile, operational safety should be ensured to avoid unexpected collisions with surroundings out of the constrained region. Our control objective is to design a controller for the manipulator, which can track the shaped virtual trajectory and can simultaneously guarantee that: 1) the end-effector of the manipulator remains in the constrained task space strictly; 2) all error signals are semiglobally uniformly ultimately bounded (SGUUB), which is defined in [56]; and 3) desired admittance relationship of the manipulator can be achieved under our proposed controller.

B. Dynamics Modeling of Manipulator System

The dynamics of an m-link manipulator system in the joint space can be described as [56]

$$\boldsymbol{M}(\boldsymbol{q})\ddot{\boldsymbol{q}} + \boldsymbol{C}(\boldsymbol{q},\dot{\boldsymbol{q}})\dot{\boldsymbol{q}} + \boldsymbol{g}(\boldsymbol{q}) = \boldsymbol{\tau} - \boldsymbol{\tau}_e \tag{1}$$

where $\boldsymbol{M}(\boldsymbol{q}) \in \mathbb{R}^{m\times m}$ denotes the inertia matrix, $\boldsymbol{C}(\boldsymbol{q},\dot{\boldsymbol{q}})\dot{\boldsymbol{q}} \in \mathbb{R}^m$ is the Coriolis and centripetal torque, $\boldsymbol{g}(\boldsymbol{q}) \in \mathbb{R}^m$ denotes the gravitational torque, $\boldsymbol{q}, \dot{\boldsymbol{q}}, \ddot{\boldsymbol{q}} \in \mathbb{R}^m$ denote the joint position, velocity, and acceleration vector, respectively, $\boldsymbol{\tau}_e \in \mathbb{R}^m$ denotes the interactive torque from human or contact environment, and $\boldsymbol{\tau} \in \mathbb{R}^m$ denotes the control input to the manipulator system.

The forward kinematic function $\boldsymbol{\Phi}(\boldsymbol{q})$ can map joint angle $\boldsymbol{q}$ to end-effector position $\boldsymbol{x}$ of the manipulator system. Therefore, $\boldsymbol{x} = \boldsymbol{\Phi}(\boldsymbol{q})$ can represent the forward kinematics of the manipulator. Differentiating the forward kinematics with respect to time, we can obtain $\dot{\boldsymbol{x}} = \boldsymbol{J}(\boldsymbol{q})\dot{\boldsymbol{q}}$, where $\boldsymbol{J}(\boldsymbol{q}) \in \mathbb{R}^{n\times m}$ denotes the Jacobian matrix in manipulator system. Based on inverse kinematics, $\dot{\boldsymbol{q}}$ and $\ddot{\boldsymbol{q}}$ can be calculated as follows:

$$\begin{aligned}\dot{\boldsymbol{q}} &= \boldsymbol{J}^{+}(\boldsymbol{q})\dot{\boldsymbol{x}}\\ \ddot{\boldsymbol{q}} &= \dot{\boldsymbol{J}}^{+}(\boldsymbol{q})\dot{\boldsymbol{x}} + \boldsymbol{J}^{+}(\boldsymbol{q})\ddot{\boldsymbol{x}}\end{aligned} \tag{2}$$

where $\boldsymbol{x} = [x_1, x_2, \ldots, x_n]^T$ is the position vector of end-effector for manipulators in the task space and n is the dimension of the end-effector coordinates. We consider the manipulators with known forward kinematic function $\boldsymbol{\Phi}(\boldsymbol{q})$ and the Jacobian matrix $\boldsymbol{J}(\boldsymbol{q}) \in \mathbb{R}^{n\times m}$ in this article. $\boldsymbol{J}^{+}(\boldsymbol{q})$ denotes the pseudoinverse matrix of $\boldsymbol{J}(\boldsymbol{q})$. $\boldsymbol{x}$, $\dot{\boldsymbol{x}}$, $\ddot{\boldsymbol{x}} \in \mathbb{R}^n$ are position, velocity, and acceleration vectors in the task space, respectively.

Substituting (2) into (1), we can obtain the dynamics of an n-dimensional manipulator system in the task space

$$\boldsymbol{M}_x(\boldsymbol{q})\ddot{\boldsymbol{x}} + \boldsymbol{C}_x(\boldsymbol{q},\dot{\boldsymbol{q}})\dot{\boldsymbol{x}} + \boldsymbol{g}_x(\boldsymbol{q}) = \boldsymbol{f} - \boldsymbol{f}_e \tag{3}$$

where $\boldsymbol{M}_x(\boldsymbol{q}) \in \mathbb{R}^{n\times n}$, $\boldsymbol{C}_x(\boldsymbol{q},\dot{\boldsymbol{q}}) \in \mathbb{R}^{n\times n}$, and $\boldsymbol{g}_x(\boldsymbol{q}) \in \mathbb{R}^n$ denote the inertia matrix, Coriolis and centripetal matrix, and gravity vector in the task space, respectively. $\boldsymbol{f}_e \in \mathbb{R}^n$ denotes external force, which is 0, when there is no contact between end-effector of manipulator and human or environment, and $\boldsymbol{f} \in \mathbb{R}^n$ denotes the control input to the manipulator. These matrices and vectors can be calculated as follows:

$$\begin{aligned}\boldsymbol{M}_x(\boldsymbol{q}) &= \boldsymbol{J}^{+T}(\boldsymbol{q})\boldsymbol{M}(\boldsymbol{q})\boldsymbol{J}^{+}(\boldsymbol{q})\\ \boldsymbol{C}_x(\boldsymbol{q},\dot{\boldsymbol{q}}) &= \boldsymbol{J}^{+T}(\boldsymbol{q})(\boldsymbol{C}(\boldsymbol{q},\dot{\boldsymbol{q}}) - \boldsymbol{M}(\boldsymbol{q})\boldsymbol{J}^{+}(\boldsymbol{q})\dot{\boldsymbol{J}}(\boldsymbol{q}))\boldsymbol{J}^{+}(\boldsymbol{q})\\ \boldsymbol{g}_x(\boldsymbol{q}) &= \boldsymbol{J}^{+T}(\boldsymbol{q})\boldsymbol{g}(\boldsymbol{q})\\ \boldsymbol{f} &= \boldsymbol{J}^{+T}(\boldsymbol{q})\boldsymbol{\tau}\\ \boldsymbol{f}_e &= \boldsymbol{J}^{+T}(\boldsymbol{q})\boldsymbol{\tau}_e.\end{aligned} \tag{4}$$

Remark 1: In this article, all the control tasks are designed and achieved in the task space. It will be more convenient to design the controller for pHRI in the task space directly. Therefore, it is necessary to transform the dynamics of a manipulator in the joint space into the dynamics in the task space.

C. Radial Basis Function Neural Network

RBFNN is commonly utilized to estimate uncertainties in model dynamics, which contains three layers, i.e., the input layer, the hidden layer, and the output layer. RBFNN belongs to linear parameterized NNs, which can be shown as follows [61]:

$$H_i(\boldsymbol{Z}) = \boldsymbol{W}_i^T\boldsymbol{S}_i(\boldsymbol{Z}), \quad i = 1, 2, \ldots, \upsilon \tag{5}$$

where $\boldsymbol{Z} = [z_1, z_2, \ldots, z_p] \in \mathbb{R}^p$ denotes the input vectors, p is the dimension of $\boldsymbol{Z}$, υ is the total number of RBFNN, $\boldsymbol{W}_i = [w_1, w_2, \ldots, w_l]^T \in \mathbb{R}^l$ denotes weight vectors in NNs, l is the number of RBFNN nodes, $\boldsymbol{S}_i(\boldsymbol{Z}) = [s_1(\boldsymbol{Z}), s_2(\boldsymbol{Z}), \ldots, s_l(\boldsymbol{Z})]^T \in \mathbb{R}^l$ denotes the basis functions, and $s_j(\boldsymbol{Z})$, $j = 1, 2, \ldots, l$ denotes neuron activation functions.

RBFNN is a particular network that uses the Gaussian radial basis functions as the basis functions

$$s_j(\boldsymbol{Z}) = \exp\left[\frac{-(\boldsymbol{Z}-\boldsymbol{o}_j)^T(\boldsymbol{Z}-\boldsymbol{o}_j)}{\varsigma_j^2}\right], \quad j = 1, 2, \ldots, l \tag{6}$$

where $\boldsymbol{o}_j = [o_{j1}, o_{j2}, \ldots, o_{jp}]^T$ is the centers of the receptive field and ς_j is the Gaussian function's widths. There exist optimal weights $\boldsymbol{W}_i^*$, which yields

$$H_i(\boldsymbol{Z}) = \boldsymbol{W}_i^{*T}\boldsymbol{S}_i(\boldsymbol{Z}) + \epsilon_i \tag{7}$$

where ϵ_i is the approximation errors. The ideal weight vectors $\boldsymbol{W}_i^*$ is an artificial quantities for analytical purposes, which is defined as the value of $\boldsymbol{W}_i$ that minimizes $|\epsilon_i|$

$$\boldsymbol{W}_i^* = \arg\min_{\boldsymbol{W}_i \in R^l}\{\sup_{\boldsymbol{Z}\in\Omega_{\boldsymbol{Z}}}|\epsilon_i|\}. \tag{8}$$

D. Useful Properties, Assumptions, and Lemmas

Property 1: The inertia matrices $\boldsymbol{M}(\boldsymbol{q})$ and $\boldsymbol{M}_x(\boldsymbol{q})$ are symmetric positive definite [56].

Property 2: The matrix $\dot{\boldsymbol{M}}_x(\boldsymbol{q}) - 2\boldsymbol{C}_x(\boldsymbol{q}, \dot{\boldsymbol{q}})$ is skew symmetric [56].

Assumption 1: For the desired trajectory vectors $\boldsymbol{x}_d = [x_{d_1}, x_{d_2}, \ldots, x_{d_n}]^T$ and constraints k_{c_i}, $i = 1, 2, \ldots, n$, there exist positive constants k_{d_i}, $i = 1, 2, \ldots, n$, such that $|\, x_{d_i}\,| \leq k_{d_i} < k_{c_i} \forall t \geq 0$.

Assumption 2: There exists a positive constant $\bar{f}_e$ such that $\|\boldsymbol{f}_e\| \leq \bar{f}_e \forall t \geq 0$ [56].

Lemma 1 [62]: For any constants k_{c_i}, $i = 1, 2, \ldots, n$, let $\chi := \{\boldsymbol{x} \in \mathbb{R}^n : |\, x_i(t)\,| < k_{c_i},\ i = 1, 2, \ldots, n, t \geq 0\} \subset \mathbb{R}^n$ and $\aleph := \mathbb{R}^l \times \chi \subset \mathbb{R}^{l+n}$ be open sets. Then, consider the system as follows:

$$\dot{\eta} = h(t, \eta) \tag{9}$$

where $\eta := [\omega, x]^T \in \aleph$ and $h : \mathbb{R}_+ \times \aleph \to \mathbb{R}^{l+n}$ is piecewise continuous in t and locally Lipschitz in η uniformly in t, on $\mathbb{R}_+ \times \aleph$. Let $\chi_i := \{x_i \in \mathbb{R} : |\, x_i(t)\,| < k_{c_i},\ i = 1, 2, \ldots, n, t \geq 0\} \subset \mathbb{R}$. Suppose that there exist functions $U : \mathbb{R}^l \to \mathbb{R}_+$ and $V_i : \chi_i \to \mathbb{R}_+, i = 1, 2, \ldots, n$ continuously differentiable and positive definite in their respective domains, such that

$$V_i \to \infty \quad as \quad |x_i| \to k_{c_i} \tag{10}$$

$$\gamma_1(\|\omega\|) \leq U(\omega) \leq \gamma_2(\|\omega\|) \tag{11}$$

where γ_1 and γ_2 are class K_∞ functions. Let $V(\eta) := \sum_{i=1}^n V_i(x_i) + U(\omega)$ and $x_i(0) \in \chi$. If the inequality holds

$$\dot{V} = \frac{\partial V}{\partial \eta} \leq -\mu V + C \tag{12}$$

in the set $\boldsymbol{x} \in \chi$, where μ and C are positive constants, then $\boldsymbol{x}(t) \in \chi\ \forall t \in [0, \infty)$.

Lemma 2: For ensuring the output of system remaining in the constrained task space, we introduce IBLF candidate as

$$V = \sum_{i=1}^n V_i = \sum_{i=1}^n \int_0^{z_i} \frac{\rho k_{c_i}^2}{k_{c_i}^2 - (\rho + \varpi_i)^2} d\rho \tag{13}$$

where $z_i = x_i - \varpi_i$, and ϖ_i is a continuously differentiable function satisfying $|\varpi_i| < k_{c_i}, i = 1, 2, \ldots, n$. It is known that V is a continuously positive differentiable functions over the set $\{|x_i| < k_{c_i}\}$. As for $|x_i| < k_{c_i}, i = 1, 2, \ldots, n$, there is

$$\frac{z_i^2}{2} \leq V_i \leq \frac{k_{c_i}^2 z_i^2}{k_{c_i}^2 - x_i^2}. \tag{14}$$

Proof: Define

$$p_i(\rho, \varpi_i) = \frac{(\rho k_{c_i}^2)}{k_{c_i}^2 - (\rho + \varpi_i)^2} \tag{15}$$

and we can get that

$$\frac{\partial p_i(\rho, \varpi_i)}{\partial \rho} = \frac{k_{c_i}^2 - \rho^2 - \varpi_i^2}{k_{c_i}^2 - (\rho + \varpi_i)^2} \tag{16}$$

which is positive in the set $|\rho + \varpi_i| < k_{c_i}$. Since $p_i(0, \varpi_i)$ for $|\varpi_i| < k_{c_i}$ and $p_i(\rho, \varpi_i)$ is increasing with ρ in the set $|\rho + \varpi_i| < k_{c_i}$, we can easily get that

$$\int_0^{z_i} p_i(\rho, \varpi_i) d\rho \leq z_i p_i(z_i, \varpi_i) \tag{17}$$

for $|z_i + \varpi_i| < k_{c_i}$. Therefore, we can get

$$\int_0^{z_i} \frac{\rho k_{c_i}^2}{k_{c_i}^2 - (\rho + \varpi_i)^2} d\rho \leq \frac{k_{c_i}^2 z_i^2}{k_{c_i}^2 - x_i^2}. \tag{18}$$

Then, we define

$$\begin{aligned} g(z_i) &= \int_0^{z_i} \frac{\rho k_{c_i}^2}{k_{c_i}^2 - (\rho + \varpi_i)^2} d\rho - \frac{z_i^2}{2} \\ &= \int_0^{z_i} \frac{\rho(\rho + \varpi_i)^2}{k_{c_i}^2 - (\rho + \varpi_i)^2} d\rho \end{aligned} \tag{19}$$

and

$$\frac{\partial g(z_i)}{\partial z_i} = \frac{z_i x_i^2}{k_{c_i}^2 - x_i^2} \tag{20}$$

over the compact set $\{|x_i| < k_{c_i}\}$, where $k_{c_i}^2 - x_i^2 > 0$. When $z_i < 0$, we have $(\partial g(z_i)/\partial z_i) < 0$. When $z_i > 0$, we have $(\partial g(z_i)/\partial z_i) > 0$. Since $z_i = 0$, $g(z_i) = 0$. Furthermore, there is $g(z_i) > 0$ over the compact set $\{|x_i| < k_{c_i}\}$. Therefore, we can get

$$\int_0^{z_i} \frac{\rho k_{c_i}^2}{k_{c_i}^2 - (\rho + \varpi_i)^2} d\rho > \frac{z_i^2}{2}. \tag{21}$$

Combining the abovementioned analysis, Lemma 2 can be proved. ■

III. Control Design

A. Constrained Space and Reference Trajectory Shaping

To ensure interaction safety, the end-effector of the manipulator system should remain within the constrained task space all the time. We first shape the reference trajectory to ensure the reference trajectory within the constrained task space subjectively. In order to obtain the reference trajectory $\boldsymbol{x}_r$, we first consider a desired admittance model in the task space as follows:

$$\boldsymbol{M}_d\ddot{\tilde{\boldsymbol{x}}} + \boldsymbol{D}_d\dot{\tilde{\boldsymbol{x}}} + \boldsymbol{K}_d\tilde{\boldsymbol{x}} = \boldsymbol{f}_e \tag{22}$$

where $\tilde{\boldsymbol{x}} = \bar{\boldsymbol{x}}_r - \boldsymbol{x}_d$, $\bar{\boldsymbol{x}}_r$ is an intermediate variable vector, and $\boldsymbol{x}_d$ is the desired trajectory vector. $\boldsymbol{M}_d, \boldsymbol{D}_d$, and $\boldsymbol{K}_d$ are the desired inertia, damper, and stiffness matrices of the desired admittance model, respectively. $\bar{\boldsymbol{x}}_r$ can be obtained when $\boldsymbol{K}_d, \boldsymbol{D}_d, \boldsymbol{M}_d$, and $\boldsymbol{x}_d$ are available and $\boldsymbol{f}_e$ can be online measured. For simplicity, we decompose the admittance model into each dimension in the task space, and $\bar{x}_{r_i}$ can be obtained from the admittance model equation

$$K_{m_i}\ddot{\tilde{x}}_i + K_{d_i}\dot{\tilde{x}}_i + K_{k_i}\tilde{x}_i = f_{e_i}, \quad i = 1, 2, 3 \tag{23}$$

where K_{m_i}, K_{d_i}, and K_{k_i} are positive constants to guarantee the desired admittance relationship at the end-effector and $\tilde{x}_i = \bar{x}_{r_i} - x_{d_i}$. For ensuring the reference trajectory remaining in the constrained region, we obtain x_{r_i} by a soft saturation function as follows:

$$x_{r_i} = \begin{cases} \bar{x}_{r_i}, & \text{if } |\bar{x}_{r_i}| \le \eta k_{c_i} \\ -\theta_i(1 - e^{(\bar{x}_{r_i} + \eta k_{c_i})/\theta_i}) - \eta k_{c_i}, & \text{if } \bar{x}_{r_i} < -\eta k_{c_i} \\ \theta_i(1 - e^{(\eta k_{c_i} - \bar{x}_{r_i})/\theta_i}) + \eta k_{c_i}, & \text{if } \bar{x}_{r_i} > \eta k_{c_i} \end{cases} \tag{24}$$

where $i = 1, 2, 3$, $\theta_i = (1 - \eta)k_{c_i}$, and η $(0 \ll \eta < 1)$ is a constant very close to 1 and selected to satisfy

$$|x_{d_i}(t)| \le k_{d_i} < \eta k_{c_i} \quad \forall t \ge 0 \tag{25}$$

where k_{d_i} and k_{c_i} are defined in Assumption 1. It is obvious that the soft saturation function ensures x_{r_i} be twice differentiable and constrained in the task space. The soft saturation function ensures that the subjective mobile intention of robotic manipulator x_{r_i} never goes beyond the constrained boundary, and the constraint is preliminarily implemented in path planning. If x_i tracks x_{r_i} precisely, the constraints are never violated, and the admittance relationship can be achieved in the constrained task space.

B. Control Design With Output Constraint

Because human motion intention is uncertain within the constrained space during pHRI, only reference trajectory shaping cannot ensure the end-effector of robotic manipulators within the constrained space. Besides, unsatisfactory tracking performance under controller will cause large overshoot, which results in that the output of manipulator system is over constraints. Therefore, based on the reference trajectory shaping via constructing soft saturation function, other effective methods on constraining system output should be employed in controller design. In this work, IBLF is developed to ensure the output remaining in the predefined task space. To facilitate the analysis and explanation, we define $\boldsymbol{x}_1 = \boldsymbol{x}$ and $\boldsymbol{x}_2 = \dot{\boldsymbol{x}}$. The dynamics of manipulator system (3) can be rewritten in state-space form as follows:

$$\begin{aligned} \dot{\boldsymbol{x}}_1 &= \boldsymbol{x}_2 \\ \dot{\boldsymbol{x}}_2 &= \boldsymbol{M}_x(\boldsymbol{q})^{-1}(\boldsymbol{f} - \boldsymbol{f}_e - \boldsymbol{g}_x(\boldsymbol{q}) - \boldsymbol{C}_x(\boldsymbol{q}, \dot{\boldsymbol{q}})\boldsymbol{x}_2). \end{aligned} \tag{26}$$

We define error variables $\boldsymbol{z}_1$ and $\boldsymbol{z}_2$ as follows:

$$\begin{aligned} \boldsymbol{z}_1 &= \boldsymbol{x}_1 - \boldsymbol{x}_r \\ \boldsymbol{z}_2 &= \boldsymbol{x}_2 - \boldsymbol{\alpha} \end{aligned} \tag{27}$$

where $\boldsymbol{z}_1 = [z_{1_1}, z_{1_2}, \ldots, z_{1_n}]^T$, $\boldsymbol{z}_2 = [z_{2_1}, z_{2_2}, \ldots, z_{2_n}]^T$, and $\boldsymbol{\alpha} = [\alpha_1, \alpha_2, \ldots, \alpha_n]^T$ denotes the virtual control variable vectors.

One of control objectives is to maintain system output $\boldsymbol{x}_1$ be constrained in the constrained region, namely, $|x_{1_i}| < k_{c_i}, i = 1, 2, 3$. To avoid violating constraints, we consider IBLF candidate as follows:

$$V_1 = \sum_{i=1}^{n} \int_0^{z_{1_i}} \frac{\rho k_{c_i}^2}{k_{c_i}^2 - (\rho + x_{r_i})^2} d\rho. \tag{28}$$

The time derivative of V_1 yields

$$\dot{V}_1 = \sum_{i=1}^{n} \frac{z_{1_i} k_{c_i}^2}{k_{c_i}^2 - x_{1_i}^2} \dot{z}_{1_i} + \sum_{i=1}^{n} \frac{\partial V_1}{\partial x_{r_i}} \dot{x}_{r_i} \tag{29}$$

where

$$\frac{\partial V_1}{\partial x_{r_i}} = z_{1_i}\left(\frac{k_{c_i}^2}{k_{c_i}^2 - x_{1_i}^2} - \lambda_i\right) \tag{30}$$

$$\lambda_i = \frac{k_{c_i}}{2z_{1_i}} \ln \frac{(k_{c_i} + z_{1_i} + x_{r_i})(k_{c_i} - x_{r_i})}{(k_{c_i} - z_{1_i} - x_{r_i})(k_{c_i} + x_{r_i})}. \tag{31}$$

Remark 2: In (31)

$$\lim_{z_{1_i} \to 0} \frac{k_{c_i}}{2z_{1_i}} \ln \frac{(k_{c_i} + z_{1_i} + x_{r_i})(k_{c_i} - x_{r_i})}{(k_{c_i} - z_{1_i} - x_{r_i})(k_{c_i} + x_{r_i})} = \frac{k_{c_i}^2}{k_{c_i}^2 - x_{r_i}^2}.$$

Therefore, the singularity for this term will not happen.

We design the virtual control variable α_i as follows:

$$\alpha_i = -k_i z_{1_i} + \frac{\left(k_{c_i}^2 - x_{1_i}^2\right)\dot{x}_{r_i}\lambda_i}{k_{c_i}^2} \tag{32}$$

where $k_i, i = 1, 2, \ldots, n$ are positive constants. Substituting (32) into (29), we can get

$$\dot{V}_1 = -\sum_{i=1}^{n} \frac{k_i z_{1_i}^2 k_{c_i}^2}{k_{c_i}^2 - x_{1_i}^2} + \sum_{i=1}^{n} \frac{z_{1_i} z_{2_i} k_{c_i}^2}{k_{c_i}^2 - x_{1_i}^2}. \tag{33}$$

Then, we design V_2 as follows:

$$V_2 = V_1 + \frac{1}{2}\boldsymbol{z}_2^T \boldsymbol{M}_x(\boldsymbol{q})\boldsymbol{z}_2 \tag{34}$$

the derivative with time of V_2 is

$$\begin{aligned} \dot{V}_2 &= \dot{V}_1 + \boldsymbol{z}_2^T \boldsymbol{M}_x(\boldsymbol{q})\dot{\boldsymbol{z}}_2 + \frac{1}{2}\boldsymbol{z}_2^T \dot{\boldsymbol{M}}_x(\boldsymbol{q})\boldsymbol{z}_2 \\ &= -\sum_{i=1}^{n} \frac{k_i z_{1_i}^2 k_{c_i}^2}{k_{c_i}^2 - x_{1_i}^2} + \sum_{i=1}^{n} \frac{z_{1_i} z_{2_i} k_{c_i}^2}{k_{c_i}^2 - x_{1_i}^2} \\ &\quad + \boldsymbol{z}_2^T(\boldsymbol{f} - \boldsymbol{f}_e - \boldsymbol{g}_x(\boldsymbol{q}) - \boldsymbol{C}_x(\boldsymbol{q}, \dot{\boldsymbol{q}})\boldsymbol{x}_2 \\ &\quad - \boldsymbol{M}_x(\boldsymbol{q})\dot{\boldsymbol{\alpha}}) + \frac{1}{2}\boldsymbol{z}_2^T \dot{\boldsymbol{M}}_x(\boldsymbol{q})\boldsymbol{z}_2 \end{aligned} \tag{35}$$

and design the control input $\boldsymbol{f} = \boldsymbol{f}_m$ as follows:

$$\begin{aligned} \boldsymbol{f}_m = &-\begin{pmatrix} \dfrac{z_{1_1} k_{c_1}^2}{k_{c_1}^2 - x_{1_1}^2} \\ \dfrac{z_{1_2} k_{c_2}^2}{k_{c_2}^2 - x_{1_2}^2} \\ \vdots \\ \dfrac{z_{1_n} k_{c_n}^2}{k_{c_n}^2 - x_{1_n}^2} \end{pmatrix} - \boldsymbol{K}_2 \boldsymbol{z}_2 + \boldsymbol{f}_e + \boldsymbol{g}_x(\boldsymbol{q}) \\ &+ \boldsymbol{C}_x(\boldsymbol{q}, \dot{\boldsymbol{q}})\boldsymbol{\alpha} + \boldsymbol{M}_x(\boldsymbol{q})\dot{\boldsymbol{\alpha}} \end{aligned} \tag{36}$$

where the positive gain matrix $\boldsymbol{K}_2 > 0$. The model-based controller can ensure that z_1 and z_2 will converge to zero and $\boldsymbol{x}_1$ can remain in the predefined constrained space. The proof of stability is given in Appendix A. From the engineering point of view, the model-based control input (36) cannot be designed in practical applications [56]. To address the uncertainty issue in the dynamic model, RBFNN is utilized to approximate uncertainties of manipulators. RBFNN can improve the tracking precision when the manipulator system tracks $\boldsymbol{x}_r$. An adaptive NN control input is proposed as follows:

$$f = -\begin{pmatrix} \dfrac{z_{1_1} k_{c_1}^2}{k_{c_1}^2 - x_{1_1}^2} \\ \dfrac{z_{1_2} k_{c_2}^2}{k_{c_2}^2 - x_{1_2}^2} \\ \vdots \\ \dfrac{z_{1_n} k_{c_n}^2}{k_{c_n}^2 - x_{1_n}^2} \end{pmatrix} - \boldsymbol{K}_2 z_2 + \boldsymbol{f}_e + \hat{\boldsymbol{W}}^T \boldsymbol{S}(\boldsymbol{Z}) \quad (37)$$

where $\hat{\boldsymbol{W}}$ is the estimated weight of RBFNN, $\boldsymbol{S}(\boldsymbol{Z})$ denotes the basis function, and $\boldsymbol{Z} = [\boldsymbol{q}^T, \dot{\boldsymbol{q}}^T, \boldsymbol{\alpha}^T, \dot{\boldsymbol{\alpha}}^T]^T$ is the input variable. The adaptive updating laws are designed as follows:

$$\dot{\hat{\boldsymbol{W}}}_i = -\boldsymbol{\Gamma}_i (\boldsymbol{S}_i(\boldsymbol{Z}) z_{2_i} + \varphi_i \hat{\boldsymbol{W}}_i) \quad (38)$$

where $\boldsymbol{\Gamma}_i, i = 1, 2, \ldots, n$ are positive definite symmetric matrices and φ_i are small positive constants. $\hat{\boldsymbol{W}}^T \boldsymbol{S}(\boldsymbol{Z})$ is used to estimate $\boldsymbol{W}^{*T} \boldsymbol{S}(\boldsymbol{Z})$, which is defined as follows:

$$\boldsymbol{W}^{*T} \boldsymbol{S}(\boldsymbol{Z}) = \boldsymbol{g}_x(\boldsymbol{q}) + \boldsymbol{C}_x(\boldsymbol{q}, \dot{\boldsymbol{q}}) \boldsymbol{\alpha} + \boldsymbol{M}_x(\boldsymbol{q}) \dot{\boldsymbol{\alpha}} - \boldsymbol{\epsilon} \quad (39)$$

where $\boldsymbol{\epsilon}$ is approximation error and $\boldsymbol{W}^*$ is the optimal weight of RBFNN. The $\tilde{\boldsymbol{W}} = \hat{\boldsymbol{W}} - \boldsymbol{W}^*$ denotes the error of weight. The adaptive NN controller with the adaptation law can ensure that z_{1_i}, z_2, and $\tilde{\boldsymbol{W}}_i$ are SGUUB [56] and x_{1_i} can remain in the constrained task space. The analysis of stability is carried out by a new BLF candidate $V_3 = V_2 + (1/2) \sum_{i=1}^{n} \tilde{\boldsymbol{W}}_i^T \boldsymbol{\Gamma}_i^{-1} \tilde{\boldsymbol{W}}_i$. The proof of stability is given in Appendix B.

Theorem 1: For the manipulator system, given the initial conditions are bounded, the proposed controller (37) with adaptive law (38) ensures that z_{1_i}, z_2, and $\tilde{\boldsymbol{W}}_i$ are SGUUB [56] and x_{1_i} can remain in the constrained task space. The closed-loop error signals will remain within the compact sets Ω_{z_1}, Ω_{z_2}, and $\Omega_{\tilde{W}}$, respectively, and defined by

$$\Omega_{z_1} = \left\{ z_1 \in \mathbb{R}^n \mid |z_{1_i}| \leq \sqrt{H}, i = 1, 2, \ldots, n \right\} \quad (40)$$

$$\Omega_{z_2} = \left\{ z_2 \in \mathbb{R}^n \mid \|z_2\| \leq \sqrt{\frac{H}{\lambda_{\min}(\boldsymbol{M}_x(\boldsymbol{q}))}} \right\} \quad (41)$$

$$\Omega_{\tilde{W}} = \left\{ \tilde{\boldsymbol{W}} \in \mathbb{R}^{l \times n} \mid \|\tilde{\boldsymbol{W}}\| \leq \sqrt{\frac{H}{\lambda_{\min}(\boldsymbol{\Gamma}^{-1})}} \right\} \quad (42)$$

where $H = 2(V_3(0) + C_3/\mu_3)$. C_3 and μ_3 are given in (51). The proof of convergence is given in Appendix C.

Remark 3: The proposed control architecture is shown in Fig. 2. Under our proposed controller, the control objective is achieved that the manipulator can track the shaped virtual trajectory precisely in the task space via the NN learning approach, and all error signals are SGUUB, which means that the desired admittance relationship of a manipulator can be achieved. On the other hand, the controller simultaneously guarantees that the end-effector of the manipulator system remains in the constrained task space strictly by virtual trajectory shaping and IBLF method.

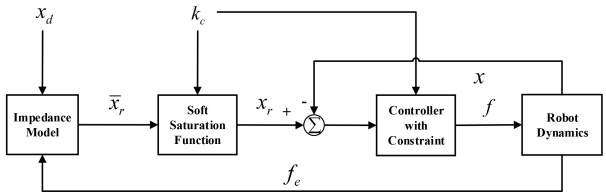

Fig. 2. Control architecture.

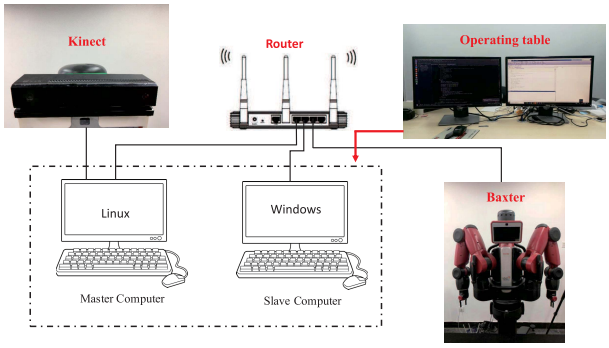

Fig. 3. Experimental platform: it is composed of the Baxter robot, Kinect camera, a master computer, and a slave computer.

IV. Experiments

In this article, the Baxter robot is employed to verify our proposed control algorithm. The robotic manipulator has seven flexible joints with advanced sensors, including position, velocity, and torque sensors. Joint sensor resolution is 14 bits with 360° (0.022° per tick resolution). Every joint can be driven by a torque controller. The designed experimental platform shown in Fig. 3 is composed of a Baxter robot, a Kinect camera, a master computer, and a slave computer.

Two computers are used in the experimental system. The master computer is employed to receive data from the Baxter robot, run main programs, and send a control command to the robot. The slave computer receives data from the master computer, calculates NN compensation, and transfers calculation results to the master computer by the user datagram protocol (UDP).

The experiment is desired to verify that the manipulator can interact with a human operator when the manipulator is operated within the constrained space obediently. In addition, the end-effector of the manipulator can remain in the constrained space to ensure safety. In this experiment, we only use the right arm of the Baxter robot and operate the robotic manipulator in the task space.

A. Design and Setting of Experiment

In the control design part, we design an adaptive NN admittance controller with output constraint and analyze the

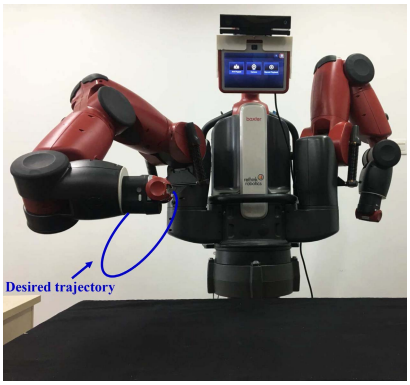

Fig. 4. Schematic of the tracking test.

stability of the system with the proposed controller by the Lyapunov method. We transform force control input $\boldsymbol{f}$ into torque input $\boldsymbol{\tau}$ in the joint torque controller as $\boldsymbol{\tau} = \boldsymbol{J}^T(\boldsymbol{q})\boldsymbol{f}$ according to (4), and $\boldsymbol{J}^T(\boldsymbol{q})$ can be obtained from ROS packages. In this part, we apply the designed torque controller on the Baxter robot to verify the proposed algorithm in experiment. Initially, the end-effector stays in the initial position $\boldsymbol{x}(0) = [-0.13(\text{m}), -0.4(\text{m}), 0.74(\text{m})]$. Control parameters are chosen as $k_1 = 17.7, k_2 = 15, k_3 = 22$, and $\boldsymbol{K}_2 = \text{diag}[5.1, 12, 4.5]$. After our repeated verification, the number of RBFNN nodes is chosen as Node $=$ 729. In these number settings, we can obtain great estimated results, and the computing time is within acceptable range. The centers of RBFNN nodes are evenly designed between the upper and lower bounds of the motion range and speed limits separately in joint space and task space in $[-1.7, 1.7] \times [-2.1, 1.0] \times [-3.1, 3.1] \times [0.0, 2.6] \times [-3.1, 3.1] \times [-1.6, 2.1] \times [-3.1, 3.1] \times [-0.5, 0.5] \times [-1, 0] \times [0.5, 1.5]$ and $[-2.0, 2.0] \times [-2.0, 2.0] \times [-2.0, 2.0] \times [-2.0, 2.0] \times [-4.0, 4.0] \times [-4.0, 4.0] \times [-4.0, 4.0] \times [-0.5, 0.5] \times [-0.5, 0.5] \times [-0.5, 0.5]$. The settings of centers can ensure the RBFNN traversing the whole joint space, task space, and operating speed space, which generates good estimated results. All initial values of RBFNN weights are set as 0. Parameters of adaptive law are $\boldsymbol{\Gamma}_i = 100\boldsymbol{I}_{\text{Node}}$ and $\varphi_i = 0.002$. The desired trajectory in the task space is described by

$$\begin{aligned} x_{d_x}(t) &= (0.15\sin(50\pi/t) - 0.1)(\text{m}) \\ x_{d_y}(t) &= (0.2\cos(50\pi/t) - 0.6)(\text{m}) \\ x_{d_z}(t) &= (0.2\sin(50\pi/t) + 0.75)(\text{m}). \end{aligned} \tag{43}$$

Then, reference trajectory $\boldsymbol{x}_r$ can be obtained by the predefined admittance model and the soft saturation function. Parameters of admittance model are designed as $k_{m_i} = 1$, $k_{d_i} = 10$ and $k_{k_i} = 30, i = 1, 2, 3$. Parameter of soft saturation function is chosen as $\eta = 0.97$, and it is obvious that $k_{d_i} = \max\{|x_{d_i}(t)|\}$.

Remark 4: In experiments, the maximum external forces are 16.5N, 24N, and 28.5N separately in the X-, Y-, and Z-axes. External forces do not exceed thresholds under normal operation. The disturbance force will not influence the experimental performance by setting stiffness parameters of the admittance model as 30 N/m.

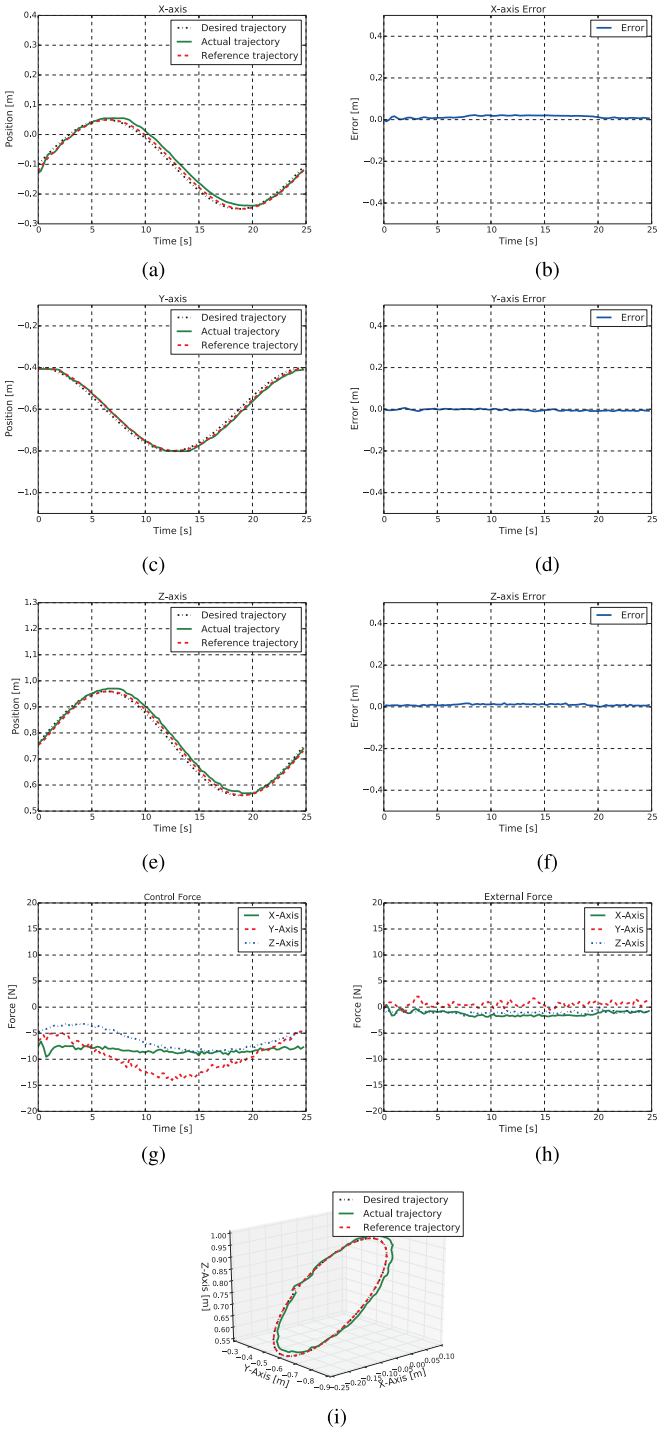

Fig. 5. Results of tracking test. (a) Tracking performance in the X-axis. (b) Tracking error in the X-axis. (c) Tracking performance in the Y-axis. (d) Tracking error in the Y-axis. (e) Tracking performance in the Z-axis. (f) Tracking error in the Z-axis. (g) Control force. (h) External force. (i) Tracking trajectory in task space.

B. Case 1: Tracking Test

In this part, we only consider the end-effector of the Baxter robot tracking the reference trajectory without interaction, as shown in Fig. 4. The tracking performances in the X-, Y-, and Z-axes are shown in Fig. 5(a), (c), and (e), where the green, red, and black lines represent the actual, reference,

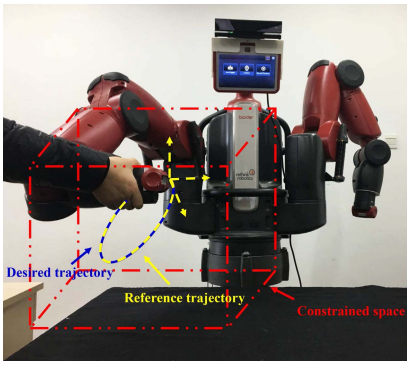

Fig. 6. Schematic of human–robot interaction within the constrained space.

and desired trajectories, respectively. The tracking error results are shown in Fig. 5(b), (d), and (f) correspondingly. The position tracking performance in the task space is shown in Fig. 5(i). It is obvious that the manipulator under our proposed controller shows a good tracking performance in real time. The reference trajectory $\boldsymbol{x}_r$ in every axis is the same as the desired trajectory $\boldsymbol{x}_d$ without interaction. The control force is shown in Fig. 5(g). External forces caused by small disturbances are near zero, which can be ignored, as shown in Fig. 5(h). It shows that the neural learning approach can solve uncertainties in the dynamics of the manipulator system, whose results are in good tracking performance.

C. Case 2: Human–Robot Interaction Test Within the Constrained Space

In this part, the robotic manipulator interacts with a human operator to perform tasks collaboratively. The control objective is to make the robotic manipulator comply with the human operator and within the predefined constrained space, as shown in Fig. 6. Constraints are set as $k_{c_1} = 0.3(\text{m})$, $k_{c_2} = 1(\text{m})$, and $k_{c_3} = 1.2(\text{m})$ in each dimension, respectively. The human operates the manipulator toward constrained boundaries in the X-, Y-, and Z-axes orderly. The tracking performances in the X-, Y-, and Z-axes are shown in Fig. 7(a), (c), and (e), where the green, red, black, and blue lines represent the actual, reference, desired trajectories, and constraint, respectively. The tracking errors in three axes converge to zero indicated in Fig. 7(b), (d), and (f), correspondingly. The position tracking performance in the task space is shown in Fig. 7(i). It is obvious that the reference trajectory $\boldsymbol{x}_r$ varies with the external force. According to the admittance model and the soft saturation function, the reference trajectory is obtained to comply with the mobile intention of humans and maintain the end-effector within the constrained boundary. The abovementioned results demonstrate that our proposed controller ensures the end-effector tracking the reference trajectory in real time within the constrained space. As shown in Fig. 7(g), control forces in three axes are in proper values whether there is an interaction or not during the task. As shown in Fig. 7(h), interaction forces in three axes are in proper values, which will not bring uncomfortable feelings to human operators. Based

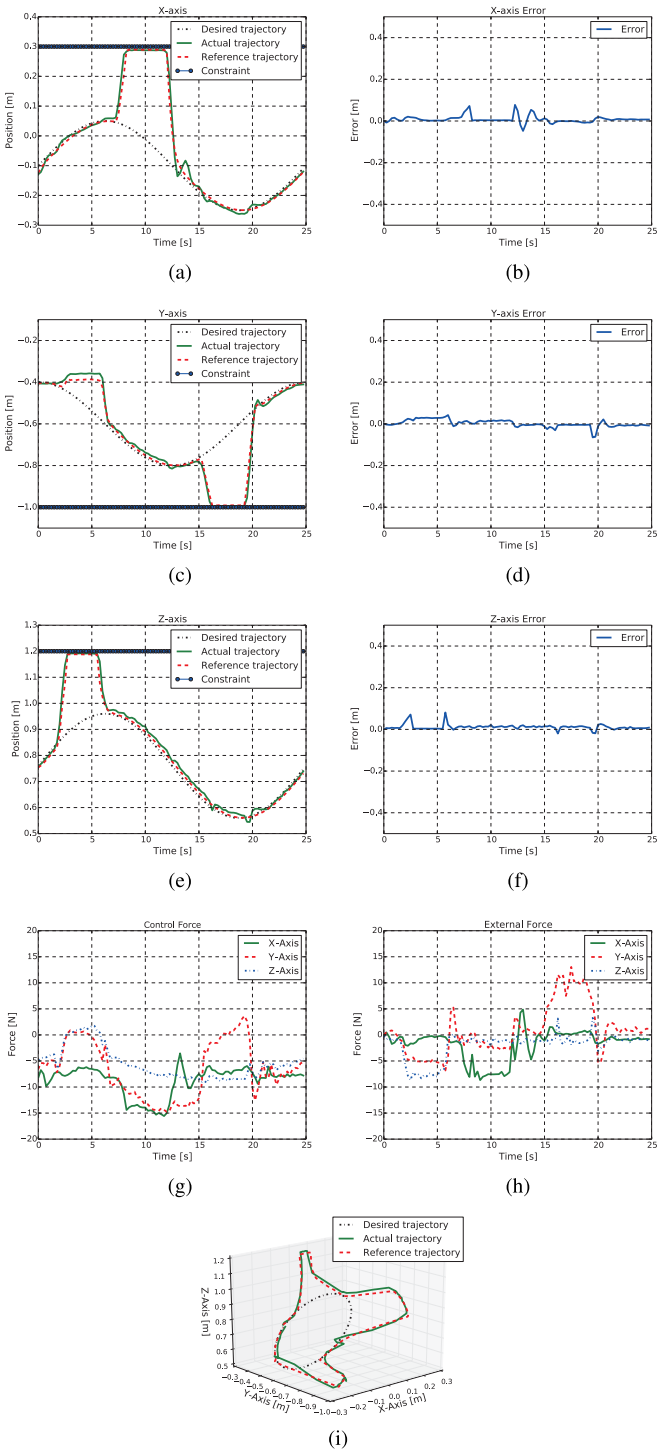

Fig. 7. Results of human–robot interaction test within the constrained space. (a) Tracking trajectory and constraint in the X-axis. (b) Tracking error in the X-axis. (c) Tracking trajectory and constraint in the Y-axis. (d) Tracking error in the Y-axis. (e) Tracking trajectory and constraint in the Z-axis. (f) Tracking error in the Z-axis. (g) Control force. (h) External force. (i) Tracking trajectory in task space.

on the results, we can give a summary that our proposed controller can ensure the end-effector of Baxter robot not only tracking the reference trajectory in a good performance but also complying with the human in the constrained task space.

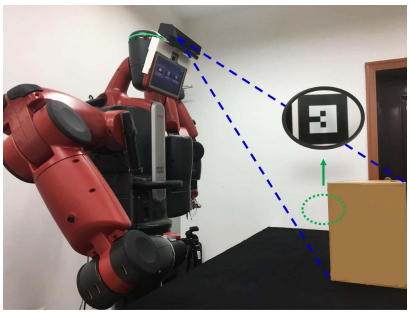

Fig. 8. Obtaining constrained boundary by a Kinect camera.

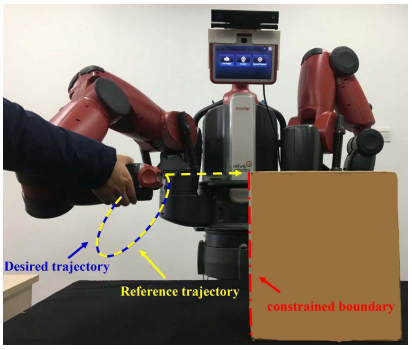

Fig. 9. Schematic of human–robot interaction within constrained space to avoid collision.

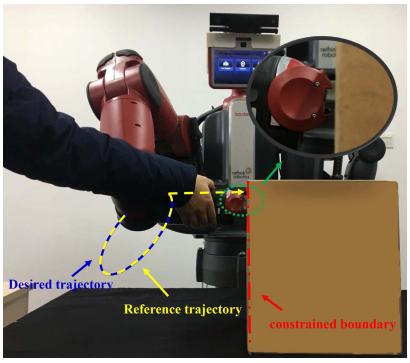

Fig. 10. Experimental results within constrained space to avoid collision.

D. Case 3: Human–Robot Interaction Test Within the Constrained Space to Avoid Collisions

In this part, the Kinect camera and quick response (QR) code are utilized to get the obstacle location, and we transfer the obtained data to the master computer. The obstacle location at the Kinect coordinate system can be transformed to the coordinate at the Baxter coordinate system through a transformation matrix. We place the Kinect on the head of the Baxter robot and paste a QR code on the edge of the obstacle so that the Kinect camera can obtain the position information of the obstacle that is in front of the Baxter robot, as shown in Fig. 8. For simplicity, we only avoid collisions in the X-axis and do not consider the constraint in the Y- and Z-axes in this experiment. Using our proposed method, we get the constrained boundary in the X-axis, $k_{c_1} = 0.35$m, in advance by the Kinect camera and common

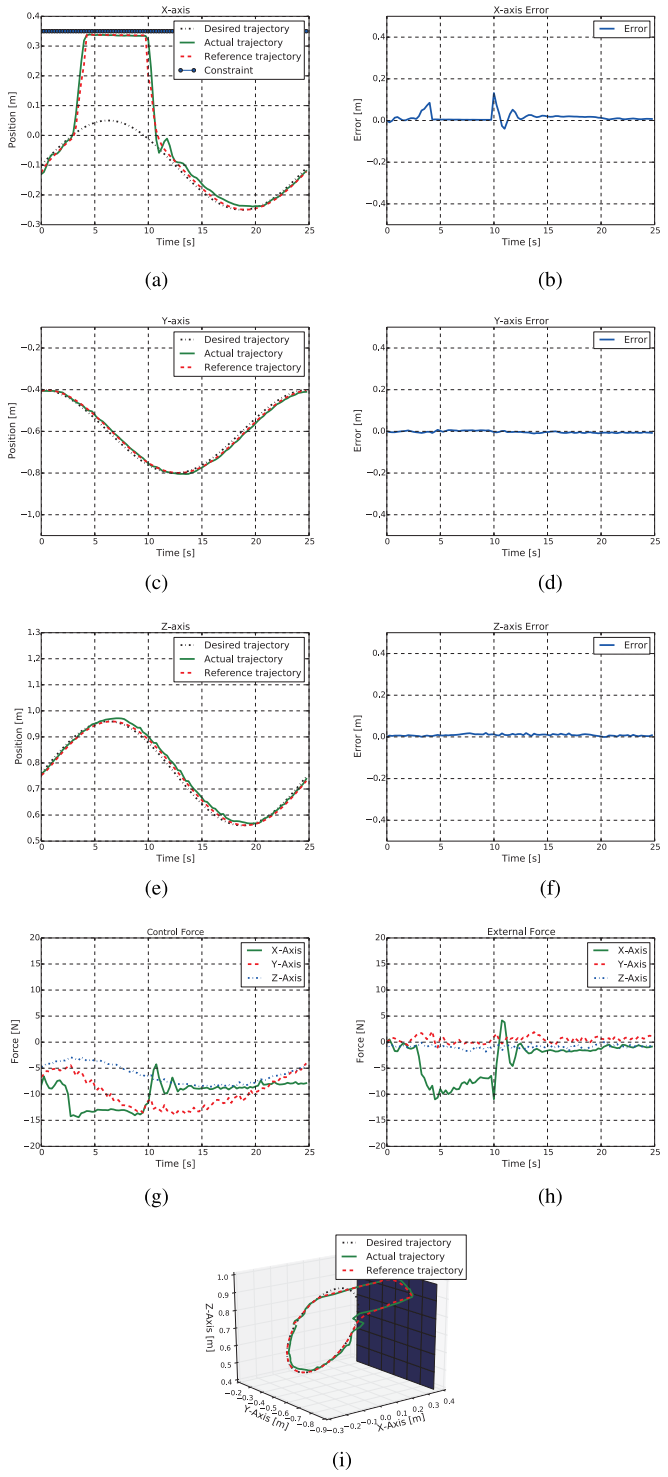

Fig. 11. Results of human–robot interaction test within the constrained space to avoid collision. (a) Tracking trajectory and constraint in the X-axis. (b) Tracking error in the X-axis. (c) Tracking trajectory and constraint in the Y-axis. (d) Tracking error in the Y-axis. (e) Tracking trajectory and constraint in the Z-axis. (f) Tracking error in the Z-axis. (g) Control force. (h) External force. (i) Tracking trajectory in task space.

filtering algorithm. In other words, our control objective in this experimental part is that the end-effector of the Baxter robot cannot beyond the constrained boundary in the X-axis to avoid collisions with an obstacle. As shown in Fig. 9, the human

operator interacts with the end-effector of the Baxter robot and moves it toward the obstacle. The experiment results are shown in Fig. 10. We can see that the end-effector cannot be operated beyond the constrained boundary under our proposed controller. Larger interaction force cannot drive the robot colliding with the obstacle either. The tracking performances of the X-, Y-, and Z-axes are shown in Fig. 11(a), (c), and (e), where the green, red, black, and blue lines represent the actual, reference, desired trajectories, and constrained boundary, respectively. The tracking error results are shown in Fig. 11(b), (d), and (f) correspondingly. It is similar to Case 2 that the reference trajectory varies with the external force in the X-axis. According to the admittance model and the soft saturation function, the reference trajectory is obtained to comply with the mobile intention of humans and keep the end-effector within the constrained boundary. It is obvious that the end-effector of the Baxter robot is constrained within the constrained boundary to avoid collisions with the obstacle. In this experiment, because of no interaction in the Y- and Z-axes, the reference trajectories $\boldsymbol{x}_r$ on these axes are the same as the desired trajectory $\boldsymbol{x}_d$. The position trajectory performance in the task space is shown in Fig. 11(i), where the blue plane respects the obstacle. As shown in Fig. 11(g), control forces in three axes are in proper values whether there is an interaction or not during the task. The interaction force is shown in Fig. 11(h), which will not bring uncomfortable feelings to human operators. Based on the results, we can give a summary that the proposed method can ensure operated safety during the process of pHRI, and the end-effector of the robotic manipulator can avoid the obstacle successfully in the task space to rely on the additional visual sensory information.

E. Conclusion of Experiments

Based on the abovementioned analysis and compared experimental results, we can conclude that the proposed control algorithm can ensure the end-effector of the manipulator complying with operators and ensure the operation safety. It has great performances of tracking and complying when the manipulator is operated within the constrained task space. We can draw the conclusion that the end-effector of the Baxter robot does not exceed the constrained space, and collisions can be avoided relying on visual feedback under our proposed controller design. The achieved admittance relationship makes the end-effector of the Baxter robot reflect compliance in pHRI.

V. Conclusion

In this article, a shaping reference trajectory by a soft saturation function has been designed in path planning. An admittance-based controller involving IBLF has been applied in pHRI, and the RBFNN learning method has been proposed to approximate dynamic uncertainties. Our proposed controller guaranteed the end-effector of the manipulator in the constrained task space and improved the compliance of interaction. The effectiveness has been verified on the Baxter robot experiment platform in three cases. In our future work, we will further research on the redundancy problem of the manipulator and focus on time-varying constrained BLF methods. We will also try to propose an advanced controller for pHRI to avoid collisions in a dynamical scenario where the obstacle position is time-varying.

Appendix A

Proof: Substituting (32) and (36) into (35), we can get

$$\dot{V}_2 = -\sum_{i=1}^{n} \frac{k_i z_{1_i}^2 k_{c_i}^2}{k_{c_i}^2 - x_{1_i}^2} - z_2^T \boldsymbol{K}_2 z_2. \tag{44}$$

Considering Lemma 2, we can get

$$\begin{aligned} \dot{V}_2 &\leq -\sum_{i=1}^{n} \int_0^{z_{1_i}} \frac{\rho k_i k_{c_i}^2}{k_{c_i}^2 - (\rho + x_{r_i})^2} d\rho - z_2^T \boldsymbol{K}_2 z_2 \\ &\leq -\mu_2 V_2 \end{aligned} \tag{45}$$

where μ_2 is a constant defined as

$$\mu_2 = \min\left(\min_{i=1,2,\ldots,n}(k_i), \frac{2\lambda_{\min}(\boldsymbol{K}_2)}{\lambda_{\max}(\boldsymbol{M}_x(\boldsymbol{q}))} \right). \tag{46}$$

To ensure $\mu_2 > 0$, control parameters k_i and positive gain matrix $\boldsymbol{K}_2$ should be satisfied

$$\min(k_i) > 0, \quad \lambda_{\min}(\boldsymbol{K}_2) > 0, \ i = 1, 2, \ldots, n.$$

It is obvious that V_2 will converge to zero. Hence, z_1 and z_2 will converge to zero, and $\boldsymbol{x}_1$ can remain in the predefined constrained space according to Lemma 1. ■

Appendix B

Proof: To prove the stability of the close-loop system, we construct a new IBLF candidate V_3 as follows:

$$V_3 = V_2 + \frac{1}{2} \sum_{i=1}^{n} \tilde{\boldsymbol{W}}_i^T \boldsymbol{\Gamma}_i^{-1} \tilde{\boldsymbol{W}}_i \tag{47}$$

where $\tilde{\boldsymbol{W}} = \hat{\boldsymbol{W}} - \boldsymbol{W}^*$ denotes the errors of weights; then, differentiating V_3 yields

$$\begin{aligned} \dot{V}_3 = &-\sum_{i=1}^{n} \frac{k_i z_{1_i}^2 k_{c_i}^2}{k_{c_i}^2 - x_{1_i}^2} + \sum_{i=1}^{n} \frac{z_{1_i} z_{2_i} k_{c_i}^2}{k_{c_i}^2 - x_{1_i}^2} \\ &+ z_2^T (\boldsymbol{f} - \boldsymbol{f}_e - \boldsymbol{g}_x(\boldsymbol{q}) - \boldsymbol{C}_x(\boldsymbol{q}, \dot{\boldsymbol{q}})\boldsymbol{\alpha} - \boldsymbol{M}_x(\boldsymbol{q})\dot{\boldsymbol{\alpha}}) \\ &+ \sum_{i=1}^{n} \tilde{\boldsymbol{W}}_i{}^T \boldsymbol{\Gamma}_i^{-1} \dot{\hat{\boldsymbol{W}}}_i. \end{aligned} \tag{48}$$

Substituting (37) into $\dot{V}_3$, we obtain

$$\begin{aligned} \dot{V}_3 = &-\sum_{i=1}^{n} \frac{k_i z_{1_i}^2 k_{c_i}^2}{k_{c_i}^2 - x_{1_i}^2} - z_2^T \boldsymbol{K}_2 z_2 \\ &+ z_2^T (\hat{\boldsymbol{W}}^T \boldsymbol{S}(\boldsymbol{Z}) - \boldsymbol{W}^{*T} \boldsymbol{S}(\boldsymbol{Z}) - \boldsymbol{\epsilon}) \\ &- \sum_{i=1}^{n} \tilde{\boldsymbol{W}}_i^T (\boldsymbol{S}_i(Z) z_{2_i} + \varphi_i \hat{\boldsymbol{W}}_i). \end{aligned} \tag{49}$$

Since inequality relation

$$\begin{aligned} -z_2{}^T \boldsymbol{\epsilon} &\leq \frac{1}{2} z_2{}^T z_2 + \frac{1}{2} \|\bar{\boldsymbol{\epsilon}}\|^2 \\ -\varphi_i \tilde{\boldsymbol{W}}_i{}^T \hat{\boldsymbol{W}}_i &\leq \frac{\varphi_i}{2} (\|\boldsymbol{W}_i{}^*\|^2 - \|\tilde{\boldsymbol{W}}_i\|^2) \end{aligned}$$

where $\|\boldsymbol{\epsilon}\| \leq \|\bar{\boldsymbol{\epsilon}}\|$, $\bar{\boldsymbol{\epsilon}}$ is the upper limit of error. We further have

$$\begin{aligned}\dot{V}_3 \leq & -\sum_{i=1}^{n}\int_0^{z_{1_i}} \frac{\rho k_i k_{c_i}^2}{k_{c_i}^2-(\rho+x_{1_i})^2}d\rho - z_2^T\left(\boldsymbol{K}_2-\frac{1}{2}\boldsymbol{I}\right)z_2 \\ & -\sum_{i=1}^{n}\frac{\varphi_i}{2}\|\tilde{\boldsymbol{W}}_i\|^2+\sum_{i=1}^{n}\frac{\varphi_i}{2}\|\boldsymbol{W}_i{}^*\|^2+\frac{1}{2}\|\bar{\boldsymbol{\epsilon}}\|^2 \\ \leq & -\mu_3 V_3 + C_3 \end{aligned} \tag{50}$$

where

$$\begin{aligned}\mu_3 = & \min\left(\min_{i=1,2,\ldots,n}(k_i), \frac{2(\lambda_{\min}(\boldsymbol{K}_2-\frac{1}{2}\boldsymbol{I}))}{\lambda_{\max}(\boldsymbol{M}_x(\boldsymbol{q}))}, \right. \\ & \left. \min_{i=1,2,\ldots,n}\left(\frac{\varphi_i}{\lambda_{\max}\left(\boldsymbol{\Gamma}_i^{-1}\right)}\right)\right) \\ C_3 = & \sum_{i=1}^{n}\frac{\varphi_i}{2}\|\boldsymbol{W}_i{}^*\|^2+\frac{1}{2}\|\bar{\boldsymbol{\epsilon}}\|^2. \end{aligned} \tag{51}$$

To ensure $\mu_3 > 0$, gain parameters k_i, positive gain matrix $\boldsymbol{K}_2$, and φ_i should be chosen to satisfy

$$\min(k_i)>0, \quad \lambda_{\min}\left(\boldsymbol{K}_2-\frac{1}{2}\boldsymbol{I}\right)>0, \quad \min(\varphi_i)>0, \quad i=1,2,\ldots,n.$$

■

APPENDIX C

Proof: Multiplying (50) by $e^{\mu_3 t}$ yields

$$\dot{V}_3 e^{\mu_3 t} \leq -\mu_3 V_3 e^{\mu_3 t} + C_3 e^{\mu_3 t} \tag{52}$$

$$\frac{d}{dt}(V_3 e^{\mu_3 t}) \leq C_3 e^{\mu_3 t}. \tag{53}$$

Integrating the abovementioned inequality, we obtain

$$\begin{aligned} & V_3 e^{\mu_3 t} - V_3(0) \\ & \quad \leq \frac{C_3}{\mu_3}e^{\mu_3 t} - \frac{C_3}{\mu_3} \end{aligned} \tag{54}$$

$$V_3 \leq \left(V_3(0)-\frac{C_3}{\mu_3}\right)e^{-\mu_3 t} + \frac{C_3}{\mu_3} \leq V(0) + \frac{C_3}{\mu_3}. \tag{55}$$

Therefore, we have

$$\frac{1}{2}|z_{1_i}|^2 \leq V_3(0) + \frac{C_3}{\mu_3}. \tag{56}$$

Hence, z_{1_i} converges to the compact set Ω_{z_1}. Bounds for $\boldsymbol{z}_2$ and $\tilde{\boldsymbol{W}}_i$ can be proven similarly. ■

ACKNOWLEDGMENT

The authors would like to sincerely thank the Editor-in-Chief, the Editor, the Associate Editor, and the anonymous reviewers for their constructive comments that helped improve the quality and presentation of this article.

REFERENCES

[1] A. U. Pehlivan, D. P. Losey, and M. K. OMalley, "Minimal assist-as-needed controller for upper limb robotic rehabilitation," *IEEE Trans. Robot.*, vol. 32, no. 1, pp. 113–124, Feb. 2016.

[2] H. Yu, S. Huang, G. Chen, Y. Pan, and Z. Guo, "Human–robot interaction control of rehabilitation robots with series elastic actuators," *IEEE Trans. Robot.*, vol. 31, no. 5, pp. 1089–1100, Oct. 2015.

[3] W. He, W. Ge, Y. Li, Y.-J. Liu, C. Yang, and C. Sun, "Model identification and control design for a humanoid robot," *IEEE Trans. Syst., Man, Cybern. Syst.*, vol. 47, no. 1, pp. 45–57, Jan. 2017.

[4] Z. Li, B. Huang, A. Ajoudani, C. Yang, C.-Y. Su, and A. Bicchi, "Asymmetric bimanual control of dual-arm exoskeletons for human-cooperative manipulations," *IEEE Trans. Robot.*, vol. 34, no. 1, pp. 264–271, Feb. 2018.

[5] T. Zhang, X. Wang, X. Xu, and C. P. Chen, "GCB-Net: Graph convolutional broad network and its application in emotion recognition," *IEEE Trans. Affect. Comput.*, early access, Aug. 27, 2019, doi: 10.1109/TAFFC.2019.2937768.

[6] T. Zhang, G. Su, C. Qing, X. Xu, B. Cai, and X. Xing, "Hierarchical lifelong learning by sharing representations and integrating hypothesis," *IEEE Trans. Syst., Man, Cybern. Syst.*, 2019, doi: 10.1109/TSMC.2018.2884996.

[7] C. Yang, H. Wu, Z. Li, W. He, N. Wang, and C.-Y. Su, "Mind control of a robotic arm with visual fusion technology," *IEEE Trans. Ind. Informat.*, vol. 14, no. 9, pp. 3822–3830, Sep. 2018.

[8] Z. Li, T. Zhao, F. Chen, Y. Hu, C.-Y. Su, and T. Fukuda, "Reinforcement learning of manipulation and grasping using dynamical movement primitives for a humanoidlike mobile manipulator," *IEEE/ASME Trans. Mechatronics*, vol. 23, no. 1, pp. 121–131, Feb. 2018.

[9] Q. Shi *et al.*, "A modified robotic rat to study rat-like pitch and yaw movements," *IEEE/ASME Trans. Mechatronics*, vol. 23, no. 5, pp. 2448–2458, Oct. 2018.

[10] C. Zeng, C. Yang, and Z. Chen, "Bio-inspired robotic impedance adaptation for human-robot collaborative tasks," *Sci. China Inf. Sci.*, to be published, doi: 10.1007/s11432-019-2748-x.

[11] M. H. Raibert and J. J. Craig, "Hybrid position/force control of manipulators," *J. Dyn. Syst., Meas., Control*, vol. 103, no. 2, pp. 126–133, 1981.

[12] M. C. Yip and D. B. Camarillo, "Model-less hybrid position/force control: A minimalist approach for continuum manipulators in unknown, constrained environments," *IEEE Robot. Autom. Lett.*, vol. 1, no. 2, pp. 844–851, Jul. 2016.

[13] C. Yang, C. Zeng, P. Liang, Z. Li, R. Li, and C.-Y. Su, "Interface design of a physical human–robot interaction system for human impedance adaptive skill transfer," *IEEE Trans. Autom. Sci. Eng.*, vol. 15, no. 1, pp. 329–340, Jan. 2018.

[14] D. Heck, A. Saccon, N. van de Wouw, and H. Nijmeijer, "Guaranteeing stable tracking of hybrid position–force trajectories for a robot manipulator interacting with a stiff environment," *Automatica*, vol. 63, pp. 235–247, Jan. 2016.

[15] N. Hogan, "Impedance control: An approach to manipulation: Part II—Implementation," *J. Dyn. Syst., Meas., Control*, vol. 107, no. 1, pp. 8–16, Mar. 1985.

[16] K. Hashtrudi-Zaad and S. E. Salcudean, "Analysis of control architectures for teleoperation systems with impedance/admittance master and slave manipulators," *Int. J. Robot. Res.*, vol. 20, no. 6, pp. 419–445, Jun. 2001.

[17] M. A. Goodrich and A. C. Schultz, "Human-robot interaction: A survey," *Found. Trends Human-Computer Interact.*, vol. 1, no. 3, pp. 203–275, 2007.

[18] F. Ficuciello, L. Villani, and B. Siciliano, "Variable impedance control of redundant manipulators for intuitive human–robot physical interaction," *IEEE Trans. Robot.*, vol. 31, no. 4, pp. 850–863, Aug. 2015.

[19] F. Ficuciello, A. Romano, L. Villani, and B. Siciliano, "Cartesian impedance control of redundant manipulators for human-robot co-manipulation," in *Proc. IEEE/RSJ Int. Conf. Intell. Robots Syst.*, Sep. 2014, pp. 2120–2125.

[20] I. Ranatunga, F. L. Lewis, D. O. Popa, and S. M. Tousif, "Adaptive admittance control for Human–Robot interaction using model reference design and adaptive inverse filtering," *IEEE Trans. Control Syst. Technol.*, vol. 25, no. 1, pp. 278–285, Jan. 2017.

[21] B. Yao, Z. Zhou, L. Wang, W. Xu, Q. Liu, and A. Liu, "Sensorless and adaptive admittance control of industrial robot in physical human–robot interaction," *Robot. Comput.-Integr. Manuf.*, vol. 51, pp. 158–168, Jun. 2018.

[22] Y. Li, S. S. Ge, and C. Yang, "Learning impedance control for physical robot–environment interaction," *Int. J. Control*, vol. 85, no. 2, pp. 182–193, Feb. 2012.

[23] A. Toedtheide, E. Shahriari, and S. Haddadin, "Tank based unified torque/impedance control for a pneumatically actuated antagonistic robot joint," in *Proc. IEEE Int. Conf. Robot. Autom. (ICRA)*, May 2017, pp. 1255–1262.

[24] C. Schindlbeck and S. Haddadin, "Unified passivity-based Cartesian force/impedance control for rigid and flexible joint robots via task-energy tanks," in *Proc. IEEE Int. Conf. Robot. Autom. (ICRA)*, May 2015, pp. 440–447.

[25] H. Li, L. Wang, H. Du, and A. Boulkroune, "Adaptive fuzzy backstepping tracking control for strict-feedback systems with input delay," *IEEE Trans. Fuzzy Syst.*, vol. 25, no. 3, pp. 642–652, Jun. 2017.

[26] X. Chen, C.-Y. Su, Z. Li, and F. Yang, "Design of implementable adaptive control for micro/nano positioning system driven by piezoelectric actuator," *IEEE Trans. Ind. Electron.*, vol. 63, no. 10, pp. 6471–6481, Oct. 2016.

[27] Y. Ren, M. Chen, and J. Liu, "Bilateral coordinate boundary adaptive control for a helicopter lifting system with backlash-like hysteresis," *Sci. China Inf. Sci.*, vol. 63, no. 1, pp. 1–3, Jan. 2020.

[28] C.-B. Yan and Q. Zhao, "Analytical approach to estimate efficiency of series machines in production lines," *IEEE Trans. Autom. Sci. Eng.* , vol. 15, no. 3, pp. 1027–1040, Jul. 2018.

[29] W. He, X. He, and C. Sun, "Vibration control of an industrial moving strip in the presence of input deadzone," *IEEE Trans. Ind. Electron.*, vol. 64, no. 6, pp. 4680–4689, Jun. 2017.

[30] W. He and S. S. Ge, "Vibration control of a nonuniform wind turbine tower via disturbance observer," *IEEE/ASME Trans. Mechatronics*, vol. 20, no. 1, pp. 237–244, Feb. 2015.

[31] G. Xie, A. Shangguan, R. Fei, W. Ji, W. Ma, and X. Hei, "Motion trajectory prediction based on CNN-LSTM sequential model," *Sci. China Inf. Sci.*, to be published, doi: 10.1007/s11432-019-2761-y.

[32] C. Hou and Q. Zhao, "Optimization of Web service-based control system for balance between network traffic and delay," *IEEE Trans. Autom. Sci. Eng.*, vol. 15, no. 3, pp. 1152–1162, Jul. 2018.

[33] C. Sun and Y. Xia, "An analysis of a neural dynamical approach to solving optimization problems," *IEEE Trans. Autom. Control*, vol. 54, no. 8, pp. 1972–1977, Aug. 2009.

[34] W. He and T. Meng, "Adaptive control of a flexible string system with input hysteresis," *IEEE Trans. Control Syst. Technol.*, vol. 26, no. 2, pp. 693–700, Mar. 2018.

[35] T. Zhao, Y. Liu, Z. Li, C.-Y. Su, and Y. Feng, "Adaptive control and optimization of mobile manipulation subject to input saturation and switching constraints," *IEEE Trans. Autom. Sci. Eng.*, vol. 16, no. 4, pp. 1543–1555, 2018.

[36] Y. Wu, B. Jiang, and N. Lu, "A descriptor system approach for estimation of incipient faults with application to high-speed railway traction devices," *IEEE Trans. Syst., Man, Cybern. Syst.*, vol. 49, no. 10, pp. 2108–2118, Oct. 2019.

[37] G. Xie, L. Sun, T. Wen, X. Hei, and F. Qian, "Adaptive transition probability matrix-based parallel IMM algorithm," *IEEE Trans. Syst., Man, Cybern. Syst.*, early access, Jun. 27, 2019, doi: 10.1109/TSMC.2019.2922305.

[38] Y.-J. Liu and S. Tong, "Barrier Lyapunov functions for Nussbaum gain adaptive control of full state constrained nonlinear systems," *Automatica*, vol. 76, pp. 143–152, Feb. 2017.

[39] H. Chen, X. Li, and J. Sun, "Stabilization, controllability and optimal control of Boolean networks with impulsive effects and state constraints," *IEEE Trans. Autom. Control*, vol. 60, no. 3, pp. 806–811, Mar. 2015.

[40] J. Wu, B. Su, J. Li, X. Zhang, X. Li, and W. Chen, "Adaptive fuzzy control for full states constrained systems with nonstrict-feedback form and unknown nonlinear dead zone," *Inf. Sci.*, vol. 376, pp. 233–247, Jan. 2017.

[41] X. Yu, W. He, H. Li, and J. Sun, "Adaptive fuzzy full-state and output-feedback control for uncertain robots with output constraint," *IEEE Trans. Syst., Man, Cybern. Syst.*, early access, Feb. 3,2020, doi: 10.1109/TSMC.2019.2963072.

[42] S. Zhang, Y. Dong, Y. Ouyang, Z. Yin, and K. Peng, "Adaptive neural control for robotic manipulators with output constraints and uncertainties," *IEEE Trans. Neural Netw. Learn. Syst.*, vol. 29, no. 11, pp. 5554–5564, Nov. 2018.

[43] K. P. Tee, B. Ren, and S. S. Ge, "Control of nonlinear systems with time-varying output constraints," *Automatica*, vol. 47, no. 11, pp. 2511–2516, Nov. 2011.

[44] Y.-J. Liu, S. Lu, S. Tong, X. Chen, C. L. P. Chen, and D.-J. Li, "Adaptive control-based barrier Lyapunov functions for a class of stochastic nonlinear systems with full state constraints," *Automatica*, vol. 87, pp. 83–93, Jan. 2018.

[45] Q. Zhou, L. Wang, C. Wu, H. Li, and H. Du, "Adaptive fuzzy control for nonstrict-feedback systems with input saturation and output constraint," *IEEE Trans. Syst., Man, Cybern. Syst.*, vol. 47, no. 1, pp. 1–12, Jan. 2017.

[46] Z.-L. Tang, K. P. Tee, and W. He, "Tangent barrier Lyapunov functions for the control of output-constrained nonlinear systems," *IFAC Proc. Volumes*, vol. 46, no. 20, pp. 449–455, 2013.

[47] X. Jin, "Fault tolerant finite-time leader—Follower formation control for autonomous surface vessels with LOS range and angle constraints," *Automatica*, vol. 68, pp. 228–236, Jun. 2016.

[48] D.-P. Li and D.-J. Li, "Adaptive neural tracking control for nonlinear time-delay systems with full state constraints," *IEEE Trans. Syst., Man, Cybern., Syst.*, vol. 47, no. 7, pp. 1590–1601, Jul. 2017.

[49] Y. Zhang, J. Sun, H. Liang, and H. Li, "Event-triggered adaptive tracking control for multiagent systems with unknown disturbances," *IEEE Trans. Cybern.*, vol. 50, no. 3, pp. 890–901, Mar. 2020.

[50] G. Wu, J. Sun, and J. Chen, "Optimal linear quadratic regulator of switched systems," *IEEE Trans. Autom. Control*, vol. 64, no. 7, pp. 2898–2904, Jul. 2019.

[51] C. Sun, W. He, and J. Hong, "Neural network control of a flexible robotic manipulator using the lumped spring-mass model," *IEEE Trans. Syst., Man, Cybern. Syst.*, vol. 47, no. 8, pp. 1863–1874, Aug. 2017.

[52] M. Chen and G. Tao, "Adaptive fault-tolerant control of uncertain nonlinear large-scale systems with unknown dead zone," *IEEE Trans. Cybern.*, vol. 46, no. 8, pp. 1851–1862, Aug. 2016.

[53] M. Chen, S.-Y. Shao, and B. Jiang, "Adaptive neural control of uncertain nonlinear systems using disturbance observer," *IEEE Trans. Cybern.*, vol. 47, no. 10, pp. 3110–3123, Oct. 2017.

[54] P. Liu, Z. Zeng, and J. Wang, "Multiple Mittag–Leffler stability of fractional-order recurrent neural networks," *IEEE Trans. Syst., Man, Cybern. Syst.*, vol. 47, no. 8, pp. 2279–2288, Aug. 2017.

[55] A. Wu and Z. Zeng, "Global Mittag–Leffler stabilization of fractional-order memristive neural networks," *IEEE Trans. Neural Netw. Learn. Syst.*, vol. 28, no. 1, pp. 206–217, Jan. 2017.

[56] W. He, S. S. Ge, Y. Li, E. Chew, and Y. S. Ng, "Neural network control of a rehabilitation robot by state and output feedback," *J. Intell. Robotic Syst.*, vol. 80, no. 1, pp. 15–31, Oct. 2015.

[57] T. Wang, H. Gao, and J. Qiu, "A combined adaptive neural network and nonlinear model predictive control for multirate networked industrial process control," *IEEE Trans. Neural Netw. Learn. Syst.*, vol. 27, no. 2, pp. 416–425, Feb. 2016.

[58] W. He and Y. Dong, "Adaptive fuzzy neural network control for a constrained robot using impedance learning," *IEEE Trans. Neural Netw. Learn. Syst.*, vol. 29, no. 4, pp. 1174–1186, Apr. 2018.

[59] K. J. Hunt, D. Sbarbaro, R. Z. Bikowski, and P. J. Gawthrop, "Neural networks for control systems: A survey," *Automatica*, vol. 28, no. 6, pp. 1083–1112, 1992.

[60] A. Q. L. Keemink, H. Van Der Kooij, and A. H. A. Stienen, "Admittance control for physical human–robot interaction," *Int. J. Robot. Res.*, vol. 37, no. 11, pp. 1421–1444, 2018.

[61] S. Zhang, P. Yang, L. Kong, W. Chen, Q. Fu, and K. Peng, "Neural networks-based fault tolerant control of a robot via fast terminal sliding mode," *IEEE Trans. Syst., Man, Cybern., Syst.*, early access, Aug. 27, 2019, doi: 10.1109/TSMC.2019.2933050.

[62] K. P. Tee, S. S. Ge, and E. H. Tay, "Barrier Lyapunov functions for the control of output-constrained nonlinear systems," *Automatica*, vol. 45, no. 4, pp. 918–927, Apr. 2009.

Wei He (Senior Member, IEEE) received the B.Eng. degree in automation and the M.Eng. degree in control science and engineering from the College of Automation Science and Engineering, South China University of Technology, Guangzhou, China, in 2006 and 2008, respectively, and the Ph.D. degree in control science and engineering from the Department of Electrical and Computer Engineering, National University of Singapore, Singapore, in 2011.

He is currently a Full Professor with the School of Automation and Electrical Engineering, University of Science and Technology Beijing, Beijing, China. He has coauthored more than two books in Springer and authored or coauthored more than 100 international journal articles and conference papers. His current research interests include robotics, distributed parameter systems, and intelligent control systems.

Prof. He was a recipient of the Newton Advanced Fellowship from the Royal Society, U.K., in 2017, and the IEEE SMC Society Andrew P. Sage Best Transactions Paper Award in 2017. Since 2018, he has been the Founding Chair of the Technical Committee on Autonomous Bionic Robotic Aircraft (TC-ABRA) of the IEEE Systems, Man and Cybernetics Society. He has been serving as the Chair for the IEEE SMC Society Beijing Capital Region Chapter. He is also serving as an Associate Editor for the IEEE TRANSACTIONS ON ROBOTICS, the IEEE TRANSACTIONS ON NEURAL NETWORKS AND LEARNING SYSTEMS, the IEEE TRANSACTIONS ON CONTROL SYSTEMS TECHNOLOGY, the IEEE TRANSACTIONS ON SYSTEMS, MAN, AND CYBERNETICS: SYSTEMS, *Science China Information Sciences*, the IEEE/CAA JOURNAL OF AUTOMATICA SINICA, and *Neurocomputing*, and an Editor for the *Journal of Intelligent and Robotic Systems*.

Chengqian Xue received the B.E. degree in automation (excellence program) from the School of Advanced Engineering, University of Science and Technology Beijing, Beijing, China, in 2018, where he is currently pursuing the M.E. degree in control science and engineering with the School of Automation and Electrical Engineering.

His current research interests include adaptive neural networks' control, robotics, and human–robot interaction.

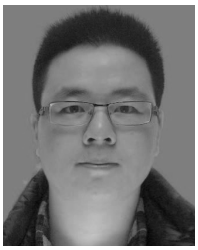

Xinbo Yu (Student Member, IEEE) received the B.E. degree in control technology and instrument from the School of Automation and Electrical Engineering, University of Science and Technology Beijing, Beijing, China, in 2013, where he is currently pursuing the Ph.D. degree in control theory and control engineering.

His current research interests include adaptive neural networks' control, robotics, and human–robot interaction.

Zhijun Li (Senior Member, IEEE) received the Ph.D. degree in mechatronics, Shanghai Jiao Tong University, Shanghai, China, in 2002.

From 2003 to 2005, he was a Post-Doctoral Fellow with the Department of Mechanical Engineering and Intelligent systems, The University of Electro-Communications, Tokyo, Japan. From 2005 to 2006, he was a Research Fellow with the Department of Electrical and Computer Engineering, National University of Singapore, Singapore, and Nanyang Technological University, Singapore. From 2017, he was a Professor with the Department of Automation, University of Science and Technology, Hefei, China. Since 2019, he has been the Vice Dean of the School of Information Science and Technology, University of Science and Technology of China, Hefei. His current research interests include wearable robotics, teleoperation systems, nonlinear control, and neural network optimization.

Dr. Li has been the Co-Chair of the IEEE SMC Technical Committee on Bio-Mechatronics and Bio-Robotics Systems (B^2S) and the IEEE RAS Technical Committee on Neuro-Robotics Systems since 2016. He has been serving as an Editor-at-Large for the *Journal of Intelligent and Robotic Systems* and an Associate Editor for several IEEE TRANSACTIONS.

Chenguang Yang (Senior Member, IEEE) received the Ph.D. degree in control engineering from the National University of Singapore, Singapore, in 2010.

He is currently a Professor of Robotics with the Bristol Robotics Laboratory, University of the West of England, Bristol, U.K. His current research interests include human–robot interaction and intelligent system design.

Prof. Yang has been awarded the EU Marie Curie International Incoming Fellowship, the U.K. EPSRC UKRI Innovation Fellowship, and the Best Paper Award of the IEEE TRANSACTIONS ON ROBOTICS, as well as over ten conference best paper awards.